

# A Somewhat Robust Image Watermark against Diffusion-based Editing Models

Mingtian Tan<sup>1</sup>, Tianhao Wang<sup>1</sup>, Somesh Jha<sup>2</sup>, and <sup>2</sup>

<sup>1</sup>University of Virginia

<sup>2</sup>University of Wisconsin Madison

**Abstract**—Recently, diffusion models (DMs) have become the state-of-the-art method for image synthesis. Editing models based on DMs, known for their high fidelity and precision, have inadvertently introduced new challenges related to image copyright infringement and malicious editing. Our work is the first to formalize and address this issue. After assessing and attempting to enhance traditional image watermarking techniques, we recognized their limitations in this emerging context. In response, we develop a novel technique, RIW (Robust Invisible Watermarking), to embed invisible watermarks leveraging adversarial example techniques. Our technique ensures a high extraction accuracy of 96% for the invisible watermark after editing, compared to the 0% offered by conventional methods. We provide access to our code<sup>1</sup>.

## 1. Introduction

Recent years have seen remarkable contributions in computer vision through advancements in image generation, largely propelled by the advent of diffusion models (DMs)[52]. This progress is partially due to their robust theoretical foundations[18], [55], enhanced latent space inference [42], and efficient image-sampling techniques [53]. These factors have led DMs to commercial success, as seen in DALL-E [40] and Stable Diffusion [42]. Additionally, DMs have spurred various emerging applications, highlighting their potential expansion in fields like data synthesis [43], video synthesis [51], [6], [59], text-to-3D synthesis [38], and image editing [7], [26], [36], [35], [4], [56].

Alongside the commercial success and potential applications of diffusion models, it also brings intellectual property (IP) concerns to the forefront [48]. Especially, the advancement of DM-based editing models [7], [26], [41], [36], due to their hyper-realistic editing effects and fundamental differences from mere image generation tasks, still presents unresolved issues of unauthorized image use and deceptive edits.

Several strategies to address these issues have been explored. For example, Liang et al. have implemented adversarial training [34], [15] to curb unauthorized style

transfer manipulation by DMs [29]. Similarly, Shan et al. introduce adversarial noise into artworks training data to hinder DMs from learning and replicating unique artistic styles [48]. Several methods embed a custom watermark in training set [67], [31] or during inference [11], [37], embedding an identifier in the produced images. Notably, the recent work Tree-Ring [58] has achieved promising results by embedding watermarks [10], [49] into the initial noise matrix of the diffusion process, thereby watermarking the model effectively.

In this paper, we investigate image watermark schemes that establish image ownership post-editing. In this field, traditional methods, such as digital [10], [49] or AutoEncoder [60], [64] based watermarks, are insufficient, especially with the advancement of DM-based image-editing models [23], because the changes introduced by modern image-editing models are unpredictable and prevalent, totally destroying the watermarks.

Our approach is to frame this as an optimization problem. Taking any target image (e.g., an artwork) and a watermark (e.g., a random image), we embed them together so that the resulting image will maintain the semantic meaning of both images in the *latent space* of the editing model. The underlying idea is to leverage the "mixup" effect [63] where multiple images can co-exist in an image (i.e., the new image is a weighted average of multiple images), and the image-editing model can operate differently on different semantics, i.e., change the target image while leaving the watermark image untouched. However, we cannot directly overlay the watermark image onto the target image, because this will make the modifications detectable. Our optimization ensures that the modifications are small.

Given the watermarked image, the next question is how to extract the watermark after it has been edited. Similar to when we embed the watermark, the watermark in the edited image should also be unnoticeable. Extracting watermarks while keeping them unnoticeable is challenging. To enhance the extraction efficacy, we propose to boost the extraction signal by embedding multiple invisible watermarks at different positions within the image, and aggregating extracted signals from those positions.

We have to limit the scope of our solution. First, we cannot defend against arbitrary edits and only focus on

1. <https://anonymous.open.science/r/RIW-2F11/>



Figure 1: For samples on editing model [7], they vary based on the text prompt where modifications are required. For instance, “Paris”, “Hong Kong”, and “Manhattan”.

minor edits (e.g., changing style, as shown in Figure 1). We argue that even non-technically, it is hard to claim IP if the image is changed significantly. Second, our method needs some knowledge about the diffusion model, but does not need access to the exact edit model or edit prompt.

Through an evaluation on two real-world datasets, the extended LAION-Aesthetics and TEDBench, as well as two state-of-the-art editing models [7], [26] from different paradigms, we discovered that, compared to prior approaches [60], [64], [10], [49], our watermarking technique demonstrates superior resistance against distortions introduced by editing models. For instance, post-editing by DMs, 96.0% of our invisible watermarks can still be extracted, while traditional methods yield a 0% success rate.

Our contributions are summarized as follows,

- We are the first to address the issues of image copyright and malicious modifications within editing models. Additionally, we formalize this problem and define our game framework.
- After assessing existing watermarking methods, we found them vulnerable to DM-based editing models. Despite our efforts using adversarial training and fine-tuning, current techniques remain inadequately prepared to tackle this new challenge.
- We propose an invisible watermarking technique, named RIW (Robust Invisible Watermarking), based on visual-semantic effects. This ensures that our watermark remains intact even after editing, addressing the image copyright issues within the editing model framework.

The rest of this paper is structured as follows: In Section 2, we review and discuss related works. In Section 3, we discuss the current editing models and the image copyright issues they introduce. We also define our threat model and discuss existing solutions. In Section 4, we refine existing techniques and introduce our approach. Section 5 gives the evaluation setup and Section 6 provides detailed experimental results. We conclude in Section 7.

## 2. Related Work

The application of semantic edits to authentic photographs or images has attracted considerable interest, particularly with the advent of advanced image synthesis techniques [14], [52], [18]. Effective image editing demands that the model excel in image generation and interpret text-based editing instructions. Numerous studies have leveraged Generative Adversarial Networks (GANs) [14] for diverse image manipulations, such as domain translation between images [21], [22], [30] or transfer the image to a specific style [1], [24], [2]. Meanwhile, with the rise of Diffusion Models (DMs) [52], we have seen even better performance in image synthesis [12], [18], [19], [45], [54] as well as other multimodal tasks such as video [51], [6], [59] and audio [27] generation.

With the advancement of DMs, concerns about image IP (Intellectual Property) have risen [52], [18], [54], [57], [33]. The realistic generative capabilities of DMs render it challenging for humans to distinguish whether images have been altered [7], [26], [41], [36], [35]. Consequently, this not only poses a threat to artwork IP but also facilitates the potential spread of misinformation through malicious image modifications. To tackle this challenge, we categorize existing solutions into two approaches: (1) safeguarding artwork samples and (2) mitigating the misuse of diffusion models (DMs).

**Safeguarding Artworks.** To shield artworks from style mimicry through diffusion Text-to-Image models [42], [44], Shan et al. introduce GLAZE [48]. It adds noise to the original artwork so that DMs like Stable Diffusion [42] and DALLE.E-m [41] cannot discern and adopt the unique art styles of these artworks. Concurrently, Liang et al. [29] launched the MIST project [28], utilizing adversarial training to incorporate noise into artworks. When these altered images are shared online, adversaries cannot obtain a high-quality image after the style transfer. Chen et al. [9] similarly add small perturbations to images to disrupt modifications.

**Mitigating Misuse of DMs.** Zhao et al. [67] propose to introduce watermarks into training samples, i.e., artworks, utilizing an AutoEncoder model [60]. Once trained on these watermarked samples, DMs consequently produce images bearing imperceptible watermarks. These watermarks can be subsequently retrieved through the decoder, establishing the ownership of public DMs. Similarly, Liu et al. employ a novel technique to watermark the latent DM [31], training their model on paired data of watermarked prompts and watermarking images. Consequently, the prompt serves as a trigger to generate their watermarked image, verifying model ownership. Contrarily, certain research takes the route of introducing watermark directly into the diffusion process [37], [58], [11], successfully extracting the watermark and leveraging the determinism inherent to the DDIM [53] generation mechanism.

### 3. Preliminaries

In this paper, we address the abovementioned issue (protecting image IP in editing models) from *a new angle using image watermarking schemes*. Specifically, we aim to add watermarks to images so that after editing, we can detect that these edited images are from those images. If adversaries malevolently alter artwork styles, infringe copyrights, or manipulate the semantic content of original images using image editing models, these watermarks can help claim ownership.

In what follows, we begin by reviewing image editing models, and then formally describe our threat model, and review existing image watermarking schemes.

#### 3.1. Image Editing

We focus on diffusion-based image editing models [35], [4], [40], [43], which show remarkable results due to the outstanding performance of Denoising Diffusion Probabilistic Models (DDPM) [18] (details deferred to Appendix A.1). Contrary to traditional GAN-based editing models such as StyleGAN [25], which are limited to singular editing functionalities (e.g., a model solely dedicated to converting facial images into smiling faces), recent DMs-based image editing models enable zero-shot editing of images merely with text instructions and achieve a superior editing quality [7], [26].

Specifically, these models typically employ an encoder  $E$  to map images (denoted by  $x$ ) into a latent space, while simultaneously mapping text edit prompts (denoted by  $p$ ) into an embedding, often using tools like CLIP [39], representing by  $C$ , due to its proficient textual understanding capabilities. Subsequently, a decoder  $D$  is used to reconstruct the high-resolution image, fusing the image and text information:

$$x_e = D[E(x), C(p)] \quad (1)$$

or more abstractly,  $x_e = \text{Edit}(x, p)$ .

#### 3.2. Problem Statement

We assume there is Alice who has access to an image-editing model, denoted by  $\text{Edit}$ , and uses it to edit images, with text prompt  $p$ . We use a subscript  $e$  to denote edition: an image  $x$  is edited into  $x_e \leftarrow \text{Edit}(x, p)$ . It is worth noting that the edition will be focused on modifying the style or changing minor things. For example, in Figure 1, the streets are changed, while the main theme stays the same. We argue that if the change can be arbitrary and the change is too much such that the whole image is changed, there is no IP issue anymore.

On the defense side, Bob embeds invisible watermarks into the images before they are published and before they are accessed by the attacker. We use  $\hat{x} \leftarrow \text{Inj}(x, w)$  to denote the injection of a watermark  $w$  into image  $x$ . Note that Bob

TABLE 1: Summary of key operations.

Party	Operations	Description
Bob	$\hat{x} \leftarrow \text{Inj}(x, w)$	Inject watermark $w$ into image $x$
Alice	$\hat{x}_e \leftarrow \text{Edit}(\hat{x}, p)$	Edit image $\hat{x}$ with text prompt $p$
Bob	$w' \leftarrow \text{Ext}(\hat{x}_e)$	Extract the watermark

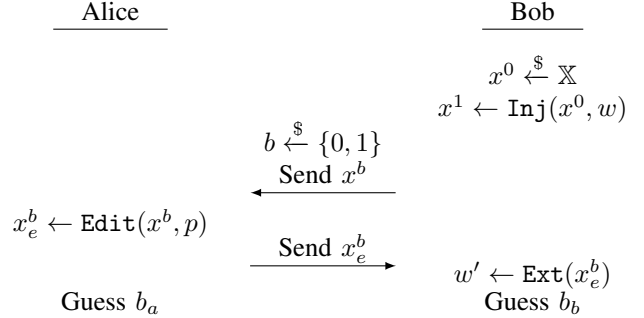


Figure 2: We formalize the problem definition into a game between Alice and Bob. Alice wins if  $b_a = b$  (Alice can detect whether there is a watermark based on  $x^b$  and  $x_e^b$ ), and Bob wins if  $b_b = b$  (Bob can extract the watermark after edits).

may have some high-level ideas about the architecture of the editing model  $\text{Edit}$ , but does not know the details of  $\text{Edit}$ , and neither can he modify  $\text{Edit}$ . Moreover, Bob has no idea what the image-editing prompt  $p$  Alice will use. After modifications by Alice, Bob can tell, and, more importantly, prove this edited watermarked image  $\hat{x}_e$  comes from the original image  $x$ . Table 1 gives the key operations.

**3.2.1. Formalizing Desired Goals.** We identify two goals in the process, which we formalize as follows.

**Invisibility.** First, the injected watermark should be invisible. Moreover, once edit models edit the watermarked images, Alice should not find out the image has been watermarked.

**Extractability.** The watermark should be robust and extractable on any edit operations (i.e., any edit model and prompt). As mentioned earlier, the modification cannot be large; otherwise, it is unclear if there are IP issues anymore. We will quantify the amount of modification later.

To capture these goals more precisely, we define a crypto-style game between Alice and Bob in Figure 2. First, Bob gets a randomly sampled image from a pre-defined set, and inserts a watermark  $w$  into it. The two images are denoted by  $x^0$  and  $x^1$ , respectively. Then one of the images  $x^b$ , where  $b$  is a random bit, is sent to Alice for editing. Then based on the edited image  $x_e^b$ , Bob tries to extract the inserted watermark. Ideally,  $w' \approx w$  only if  $b = 1$ , and in which case, Bob guesses  $b_b = 1$ ; if  $w'$  is random or is different from  $w$  Bob guesses  $b_b = 0$ . Bob wins if  $\hat{b} = b$ . At the same time, we want the watermark to be invisible.

So if Alice can distinguish if the image was watermarked or not, Alice can win. Both Alice and Bob can win at the same time, but our goal is to make only Bob win.

Our game operates in the black-box setting, i.e., Alice does not know the details about the  $\text{Inj}$  and  $\text{Ext}$  operations. On the other hand, Bob has some knowledge about the  $\text{Edit}$  operation (e.g., some publicly available edit model). We acknowledge this is a limitation of our study, and leave the exploration of the more challenging scenarios (e.g., Alice knows  $\text{Inj}$  and  $\text{Ext}$  and becomes adaptive when choosing prompts) as future work.

**3.2.2. Problem Scope.** As mentioned in related work, there has been a surge of research on knowledge copyright protection within diffusion models, categorized into *preventing* image styles from being learned by diffusion models [48], guarding against style transfers [29], and *safeguarding diffusion models* from unauthorized theft or misuse [11], [58], [67]. Our watermarking technology primarily focuses on *detecting (via watermarks)* unauthorized modifications or malicious edits of *artwork or photographs* by diffusion model-based editing tools. Artists and photographers can utilize our tool to embed subtle, nearly undetectable perturbations into their work, ensuring minimal impact on the original image quality before online publication.

The goal of our watermark is to be invisible and not to be robust against adaptive modifications: adaptive editing attack [32] or image reconstruction based on generative model [66] might remove our watermark. Also, while the game definition is flexible, in our experiment, we limit the text prompt  $p$  so that only minor changes will be made to image  $x$ . We argue that deciding whether greater change violates IP protections is a broader problem and out of the scope of this paper.

### 3.3. Existing Image Watermarking Schemes

**3.3.1. Digital Image Watermark.** Early work on image watermarking focuses on designing digital watermarks [10], [49] that integrate watermarks into colored images. Naive methods insert watermarking messages into specific locations of the image; more recent work embeds the watermark in the transformed space to make it subtle and less discernible to the human eye, but can be extracted when necessary using the inverse transformations.

**3.3.2. AutoEncoder-based Watermark.** More recently, researchers built watermarking schemes using the AutoEncoder architecture [32], [67]. In the AutoEncoder framework [60], [64], an encoder is trained to embed watermarks, while a decoder is trained for watermark extraction. Note that the encoder and decoder have similar functionalities as those defined in Equation 1, and we slightly abuse notations and reuse  $E$  and  $D$  to denote them. But the internal neural network architectures are quite different.

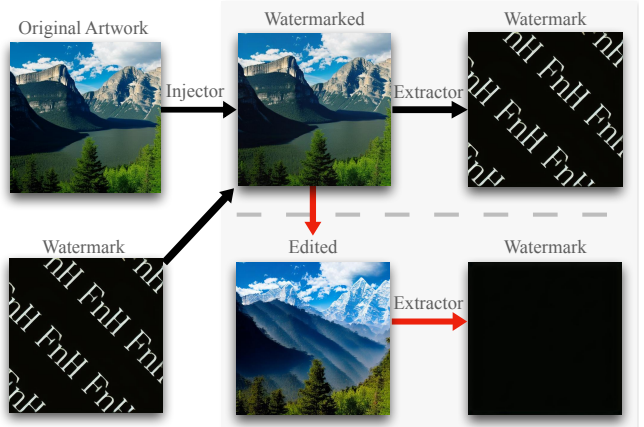


Figure 3: The example of watermarking using an AutoEncoder. The original artwork, after being watermarked by Injector  $\text{Inj}$ , can have the corresponding watermark successfully extracted by Extractor  $\text{Ext}$ . After being edited by  $\text{Instructpix2pix}$  with the text prompt “Have it be the valley of the Ten Peaks in the Himalayas”,  $\text{Ext}$  can no longer retrieve the watermark.

Specifically, an encoder  $E$  is trained as  $\text{Inj}$  to embed watermarks, while a decoder  $D$  is trained as  $\text{Ext}$  for watermark extraction. Specifically, during the embedding phase, both the image  $x$  and watermark  $w$  are fed into the  $E$  and encoded into a latent space. In this latent space, the encoder integrates the watermark and then upsamples it back to the image domain, yielding a subtly modified image  $\hat{x} \leftarrow E(x, w)$  that remains visually indistinguishable from the original format. The decoder  $D$  is then trained to extract the watermark  $w$  from  $\hat{x}$ . The optimization of the AutoEncoder is as follows,

$$\arg \min_{D, E} \|D(\hat{x}) - w\|_{\ell_2} + \lambda[\|\hat{x} - x\|_{\ell_2} + L_{\text{LPIPS}}(\hat{x}, x)] \quad (2)$$

where the first term ensures the decoder can extract the watermark  $w$  embedded by the encoder, and the second term guarantees that the watermarked image  $\hat{x}$  visually approximates the original  $x$  (by measuring similarity between  $\hat{x}$  and  $x$  using  $\ell_2$  norm and LPIPS loss [65]; but other metrics will also apply), and  $\lambda$  is used to balance the scales of these two terms.

However, our evaluations (details in Subsection 6.1) reveal that images watermarked using this method struggle to withstand distortions introduced by the edit models. As a result, it becomes challenging to extract the embedded watermark from the modified image after editing. As illustrated in Figure 3, the watermarked image  $\hat{x}$  is visually indistinguishable from the original image, and the decoder  $D$  successfully extracts the embedded watermark  $w$  from the  $\hat{x}$ . However, post-editing by image-editing models, the watermark extracted from image  $\hat{x}_e$  is difficult to see.

## 4. Our Method

We identify two fundamental flaws for the existing AutoEncoder-based watermarks: (1) they do not consider image edits, and (2) the ‘one-model-fit-all’ approach inherently makes training such a model more challenges, i.e., because the edits are so diverse, it is difficult to ensure the training converge. Overcoming the first issue is easier: we just need to redefine the objective function to incorporate image edits. On the other hand, the second issue is more fundamental, and we propose to decouple the encoding and decoding phases and consider/optimize them separately.

### 4.1. Warmup: Incorporating Image Edit

Given that the AutoEncoder-based solution is not robust against perturbations from image-editing models, we make two efforts to improve it. First, we incorporate adversarial learning [62] into the optimization objective as follows:

$$\arg \min_{D,E} \|D(\hat{x} + \alpha N) - w\|_{\ell_2} + \lambda[\|\hat{x} - x\|_{\ell_2} + L_{lpiPs}(\hat{x}, x)]$$

Compared to the original objective, here we introduce an isotropic Gaussian noise denoted by  $N$ , and  $\alpha$  represents the strength of the noise. Now  $D$  is able to extract the watermark  $w$  from images with  $\alpha$  scaled Gaussian noise, but it still fails to extract the watermark after the edited models. This is because the Gaussian noise we introduced and the diffusion process’s perturbation on the image are not exactly the same.

To address this, we further fine-tuned  $D$  using watermarked images that had been edited, and the objective function becomes

$$\arg \min_{D,E} \|D(\hat{x}_e), w\|_{\ell_2} + \lambda[\|\hat{x} - x\|_{\ell_2} + L_{lpiPs}(\hat{x}, x)] \quad (3)$$

Unfortunately, in our evaluation,  $D$  fails to fit edited images during the training process, and the training loss escalates 0%. We hypothesize that the watermark information added by  $D$  is destroyed by the editing process.

### 4.2. Watermark Injection

Having identified the difficulty of training the autoencoder, our approach decouples the watermark injection and extraction processes and consider them separately. One significant distinction from prior solutions is we formulate this process as a *per-image* optimization problem. Here the challenge is that different from training a model explicitly, we need to identify the direction of the optimization. A natural consideration is to make the watermark invisible, but then how to make sure it will be extracted later (without knowing what the extractor does)? And how to ensure the optimization is efficient?

To tackle the first question, we propose to make the watermarked image  $\hat{x}$  carries information about the watermark

$w$  in the *latent/embedding space*. That is, suppose we know the encoder  $E$  in the image-editing model (i.e.,  $E$  from Equation 1), we can ensure  $E(\hat{x})$  maintains information about  $E(w)$ , or equivalently, the distance between  $E(\hat{x})$  and  $E(x + \alpha \cdot w)$  is small, where  $\alpha$  denotes the strength of the watermark. The intuition behind working in the latent space is that image editing models typically target and modify only the instruction part, while retaining unrelated semantic information, thus retaining the watermark.

At the same time, we want to make sure  $\hat{x}$  is similar to  $x$ , as quantified earlier. We borrow the similarity measurement from previous optimization objectives, but with the LPIPS loss replaced by a post-edition invisibility penalty. Specifically, we borrow the decoder  $D$  from Stable Diffusion [42] ( $E, D$  is a pair; note that although we also use these two notations to denote the encoder and decoder of the autoencoder, their internal architectures are significantly different), which is utilized to retrieve the generated image from the latent space.  $D(E(\hat{x}))$  gives the edited watermarked image, but without any prompt. Intuitively, if  $D(E(\hat{x}))$  is similar to  $x$ , meaning that the watermark is invisible, then after the actual edition, the watermark will also be invisible. This leads to our proposed optimization objective:

$$\arg \min_{\hat{x}} \|E(\hat{x}) - E(x + \alpha \cdot w)\|_{\ell_1} + \lambda [\|\hat{x} - x\|_{\ell_2} + \|D(E(\hat{x})) - x\|_{\ell_2}] \quad (4)$$

Here the first component compares in the embedding space, and  $\ell_1$  norm is a natural metric; but like before, other metrics can also be used. We explore the interplay between  $\alpha$  and watermark detection precision in Subsection 6.3. The parameter  $\lambda$  serves as a weighting factor to balance the strength of the watermark in the latent space with the quality of image generation. Note that we employ an encoder in our optimization function similar to the target editing models. Our results indicate that this optimization approach is not relying on having identical encoders in terms of training parameters and data. By adjusting parameters  $\alpha$  and encoder loss  $\lambda$ , i.e., latent space component in the optimization objective, we can modulate the watermark’s intensity post-editing, rendering it invisible, as depicted in Figure 11a and Figure 11b.

To ensure the optimization problem is solved efficiently, we leverage and adopt the PGD [34] algorithm, which was proposed to find adversarial examples and is efficient. Our optimization process is given in Algorithm 1. Given  $x$  and  $w$ , we first obtain  $\hat{x}^0$ , and execute a series of optimization steps, in a way similar to PGD: in each step, take the sign of the gradients multiplied by a scale (intuitively a ‘learning rate’) of  $\mu$  and the change, and limit the overall change from the original sample  $x$  by  $\varepsilon$ , and update.

### 4.3. Watermark Extraction

To extract the watermark, a baseline solution is to directly calculate the pixel-wise distance between the water-

---

**Algorithm 1** Watermark Injection Pipeline

---

**Input:** Image  $x$ , transparency  $\alpha$ , watermark  $w$ , encoder  $E$ , decoder  $D$ , optimization rate  $\mu$ , upper bound  $\varepsilon$ , and number of steps  $T$ .

- 1: Define objective function  $L$  based on Equation 4
- 2: Generate target image  $x' \leftarrow x + \alpha \cdot w$
- 3: Initial watermarked sample  $\hat{x}^0 \leftarrow x'$
- 4: **for**  $t \leftarrow 0$  to  $T - 1$  **do**
- 5:    $\hat{x}^t \leftarrow \hat{x}^t + \mu \cdot \text{sgn}(\nabla_{\hat{x}^t} L(E, D, \hat{x}^t, x'))$
- 6:   Calculate  $\delta = \hat{x}^t - x$  and bound it with  $\varepsilon$  in  $\ell_1$
- 7:   Update  $\hat{x}^{t+1}$  by  $\hat{x}^t + \delta$
- 8: **end for**
- 9: **return**  $\hat{x}^T$

---

mark  $w$  and the edited image  $\hat{x}_e$ , and can claim successful extraction if the distance is below a threshold. However, we found the pixel-wise measurement is not stable in edit models, because the editions, while semantically minor, can cause a lot of pixels to be modified, potentially leading to a large pixel-wise distortion in the extracted watermark. Moreover, as our optimization goal in Equation 4 involves making the watermark invisible post-edition, this intuitively cannot work.

To overcome this issue, we propose to extract at a higher level (semantic level). Here, we propose a simple yet effective design, backed by two intuitions: (1) focus on image semantics instead of details/pixels, (2) boost accuracy by ‘divide and conquer’.

Specifically, we use simple images that are just plain text with black backgrounds as watermarks (and to differentiate, we call them text watermarks and the previous general watermark as image watermarks). For examples of text and image watermarks, refer to Figure 4 and Figure 11, respectively. This ensures the higher-level semantics of images are easier to capture (i.e., just recognize texts in the image, using off-the-shelf OCR models). We also segment the watermark into  $K$  regions, so that we will have more confidence if we can recognize texts (which can also serve as the passcode of the watermark) in most regions correctly.

#### 4.4. Discussion

To summarize, although we express our target similarly to the optimization objectives in the AutoEncoder-based solutions (for ease of understanding), the underlying technique is fundamentally different: (1) We decouple the watermark injection and extraction processes and consider them separately. (2) We formulate the watermark injection process as a *per-image* optimization problem using PGD. (3) We leverage information about the encoder and decoder and rewrite the objective to incorporate different possibilities of image edition.

The efficacy of our watermarking method is attributed to their shared foundation on Stable Diffusion [42]. Although the encoder we use during watermark optimization is not

identical to those used in the edit models, these encoders share similarities. Especially, our watermark’s resilience to distortions in the editing process is attributed to integrating the edit model’s latent space information during optimization, allowing it to convey visual semantic information similar to that of the target image in the latent space. Another potential reason is: edit models strive to preserve the original image’s semantic essence and only modify specific instruction-driven sections. We argue that due to the widespread open-source availability of generative models, such as Stable Diffusion [42], accessing similar versions of encoders is not challenging.

Although our watermark, based on visual semantic information, exhibits a higher preservation rate in the edit model, our goal is not to defend against adaptive attacks: adaptive editing attack [32] or image reconstruction based on generative model [66] might remove our watermark. We defer the exploration of such attacks to future work. Moreover, since our watermark must be imperceptible to the human eye, yet present within the latent space of the diffusion, the model optimization of  $\hat{x}$  relies on the *latent space* information of the edit model (we rely on the transferability of models and assume white-box access to an older version of the edit model in the experiment). This leads to the challenge of generating high-quality watermarks in a complete black-box scenario.

## 5. Experiment Setup

**Datasets.** We evaluate our approach using two datasets: the extended LAION-Aesthetics and TedBench. The LAION-Aesthetics has been widely used for training diffusion models [40], [7], [42], while TedBench [26] has been introduced as a benchmark dataset to measure edit models.

- LAION-Aesthetics<sup>2</sup>: Due to its large size and diverse content, the primary use of this dataset is image generation. We apply LAION-Aesthetics V2 6.5+ [47], a subset of the LAION’s 5B samples, which comprises 625K image-text pairs and includes various image types, such as paintings, digital artwork, and photographs. Brooks et al. expand the dataset to include pairs of images before and after editing, along with their corresponding edit instructions by fine-tuning GPT-3 [8] and employing the Prompt-to-Prompt [17] technique. Additionally, they apply a CLIP-based metric [7] to filter out noise like nonsensical or un-descriptive captions from this dataset, enhancing its quality and applicability.
- TEDBench<sup>3</sup>: Kavar et al. [26] have proposed TEDBench (Textual Editing Benchmark), a benchmarking dataset comprising 100 pairs of input images and target text that describe intricate non-rigid edits.

**Image Editing Model.** We utilize two state-of-the-art image editing models, i.e., Instructpix2pix [7] and

2. <http://instruct-pix2pix.eecs.berkeley.edu/>

3. <https://github.com/imagic-editing/imagic-editing.github.io/>

Imagic [26]. The design principles of these two models are entirely different: One is built as an editing model by training on a pair of images—one representing the subject to be edited and the other representing the image post-editing [7]—while the other is based on fine-tuning the model using images that require editing [26]. Both models harness the capabilities of latent space diffusion models [42] as their foundational generative framework. Detailed descriptions about these models are deferred to Appendix A.2. Additionally, the editing prompt styles for these two models are quite distinct. In *Instructpix2pix*, the edit instruction typically begins with a verb, serving as a directive, while in *Imagic*, it fully describes the post-editing image, thus guiding the model’s editing process. However, the dataset we used for evaluation, such as TEDBench [26], does not encompass both of these prompt styles. To address this, we employed the GPT-4 API to automatically transfer and generate a variety of text prompt styles, facilitating compatibility with both *Instructpix2pix* and *Imagic* model. More details refer to *Text Edit Prompt* in Appendix A.2.

**Optimization Details.** In our optimization function, we utilize the version “sd-v1-4.ckpt” for the encoder, while the edit model *Instructpix2pix* employs “sd-v1.5.ckpt” and *Imagic* uses the “sd-v1-4-full-ema.ckpt” version. Due to its fine-tuning paradigm, this model might slightly deviate from the original one. We employ the LPIPS (Learned Perceptual Image Patch Similarity) loss [65] to ensure the fidelity of our watermarked image  $\hat{x}$  in the second term of the optimization objective. All results presented in this paper are based on settings  $\varepsilon = 12/255$ ,  $\mu = 2/255$ . We set  $\lambda = 1$  in the evaluation of modification  $\alpha$ , and set  $\alpha = 0.4$  in the evaluation of modification  $\lambda$ . Appropriate adjustments of  $\lambda$  may lead to improved watermark quality, and we will explore these in future work if needed.

**Watermarks Used.** We crop the image into 9 segments/blocks, with each size (173, 66), corresponding to the nine individual watermarks  $w$  we have embedded, each consisting of four letters as seen the first example in Figure 11b.

As a baseline for comparison, we also embed the watermark in the lower right corner of the image, as shown in the first row of Figure 4. In this case, we employ images from CIFAR10 [13] as watermarks.

To differentiate the two settings, we call them *text watermarks* and *image watermarks*, respectively.

**Extraction Details.** For text watermarks, we first fine-tune MPRNet [61] to reconstruct low-resolution watermarks in edited images. Note that due to the time-consuming nature of data collection—for example, a single *Imagic* edit takes 10 minutes on an NVIDIA A100—we limited the fine-tuning of MPRNet to a dataset of 1,000 images for both *Instructpix2pix* and *Imagic*. For the second stage of our extraction process, we use an Optical Character Recognition (OCR<sup>4</sup>)-based model. For training our



Figure 4: The first row displays the target image overlaid with an image watermark, featuring a  $32 \times 32$  sized watermark in the bottom right corner (marked with a red box), randomly selected from CIFAR10 [13]. The second row showcases the invisible watermark added by our technique, and the third row illustrates the outcome post-editing of the watermarked image.

extractor Ext, we utilized additional 5,000 images from *Instructpix2pix* and 2,000 from *Imagic*.

For image watermarks, we initially compare the pixel distance between the watermarked section of the image and the *ground truth* (i.e., the selected CIFAR10 [13] image used as the watermark) for watermark recognition. Concurrently, we utilize image reconstruction technique, i.e., MPRNet, to enhance the accuracy of this method. Subsequently, we also employ a binary classification model to identify images with and without watermarks, thereby determining whether an image watermark has been added.

## 6. Evaluation Results

### 6.1. Comparison with Existing Solutions

Compared to prior watermarking methods like digital watermarks [10], [49] and AutoEncoder-based watermarks [60], [64], our approach offers notable benefits. Traditional methods yield a 0% retention in editing tasks. Given the nature of the diffusion process, especially in diffusion models (DMs) tailored for editing, watermarks from these methods face extensive distortion post-editing, rendering them unextractable.

**Digital Watermark.** We employ a popular tool<sup>5</sup> based on frequency domain techniques for inserting digital watermarks. Through evaluation, we find that the digital watermark demonstrates excellent robustness against various common image transformations such as rotation, random cropping, image masking, cutting, resizing, noise introduction, and brightness adjustment. It successfully recovers the

4. <https://github.com/clovaai/deep-text-recognition-benchmark>

5. [https://github.com/guofei9987/blind\\_watermark](https://github.com/guofei9987/blind_watermark)



Figure 5: Digital watermark examples: the first row shows the results of the original images after adding a digital watermark, rows two to four highlight traditional attacks like cropping, noise, and masking, while the last row presents post-edited images.

four-letter text watermark with 100% accuracy. However, when we subjected 100 images from LAION-Aesthetics containing the digital watermark to edits using either the `Instructpix2pix` or `Imagic` model, the accuracy for extracting the corresponding watermark dropped to zero.

Examples of digital watermarks are depicted in Figure 5, showcasing the robustness and limitations of the digital watermark. The first row exhibits original images with the applied watermark (text “Robust InvisiWater”). Subsequent rows (two to four) demonstrate the watermark’s resilience against traditional attacks like cropping, random noise, and masking, with successful extraction still possible. However, the edited images in the final row illustrate the watermark’s extraction failure. We can also observe that the impact of traditional image transformations on images is entirely different from that introduced by edit models. Furthermore, our analysis revealed that digital watermarks exhibit less resistance to brightness and rotation alterations than expected. A mere 15-degree rotation or a 1.2-fold increase in brightness rendered the watermark extraction unfeasible.

**AutoEncoder-based Watermark.** Given the popularity of utilizing AutoEncoders for watermarking tasks [60], [64], particularly in recent work that employs AutoEncoder to add watermarks to diffusion models [67], we also evaluate

TABLE 2: Time (seconds) required by various watermarking methods to add watermarks to individual images. And pre-training or auxiliary needs for each method.

Watermark Tool	Digital	AutoEncoder	Ours
Time Cost (s)	0.85	0.42	95.03
Training-Free	✓	✗	✓

a paired Encoder-Decoder<sup>6</sup> scheme in our study, i.e.,  $E$  and  $D$ . For this evaluation, we selected 10,000 images from the LAION-Aesthetics dataset and generated 5,000 three-letter random text watermarks for training the AutoEncoder.

We evaluate both `Imagic` and `Instructpix2pix` models on 100 images, the decoder  $D$  extracts watermarks with 100% accuracy from unedited images. However, this accuracy plummets to 0% post-editing. To enhance  $D$ ’s resilience against such manipulations, we employ adversarial training techniques aimed at improving  $D$ ’s ability to extract watermarks from perturbed images. However, the watermarks added to the images by the  $E$  were not retained following the editing process, resulting in 0% extraction accuracy. In addition, we attempt to *fine-tune* the  $D$  that had undergone adversarial training, using images that had been edited by both `Imagic` and `Instructpix2pix` models. A total of 1000 images were used for this purpose, with 500 images from each model. Despite the fine-tuning, there was no observable improvement in extraction accuracy, remaining 0%.

**Running Time Comparison.** In our evaluation, we assess the time overhead for watermarking an individual image using different methods, as detailed in Table 2. Notably, the AutoEncoder algorithm shows the least time overhead for watermarking. However, this does not include its substantial training time, where we spent approximately 7 hours training it on a dataset of 10,000 images using two NVIDIA A100 GPUs. In contrast, our watermarking method, though more time-consuming due to a 400-step optimization procedure, requires no additional training, data collection and pre-processing. This allows our method to be directly applied to any image without the need for preliminary steps.

## 6.2. Results of Image Watermarks

We opt to use images from CIFAR10 [13] as watermarks primarily due to their widespread use in visual tasks. Extending this rationale, CIFAR10’s diverse and representative image set offers a robust basis for watermarking, ensuring that our technique can be generalized across various image types and applications. In emulating traditional backdoor attack [16], we strategically place the watermark in the lower right corner, a choice driven by the need for subtlety and reduced visibility. This positioning not only makes the watermark less conspicuous but also leverages the typical

6. <https://github.com/yunqing-me/WatermarkDM>

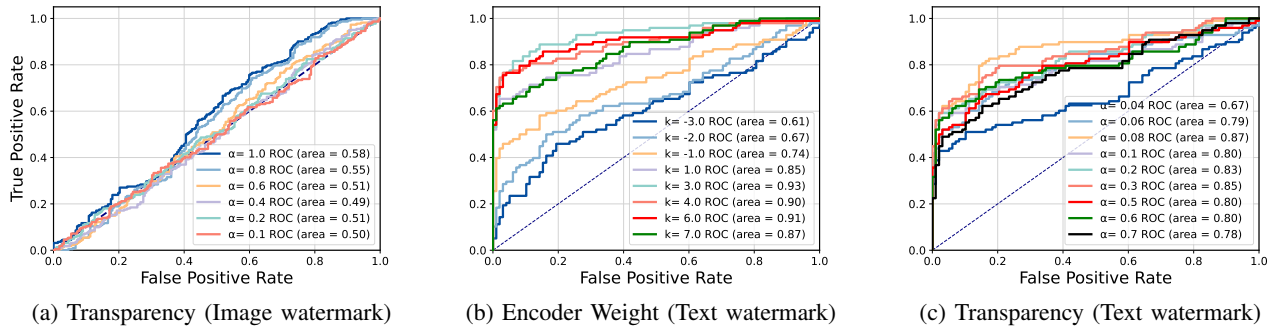


Figure 6: ROC results on the LAION-Aesthetics dataset and `Instructpix2pix` editing model. In Figure (a), we evaluate the ROC curve for naive (pixel comparison-based) extraction of image watermarking with different transparency levels  $\alpha$ . The clearer the image watermark is (less invisible), the better the classification results. Text watermarking (with  $D_{\text{letter}}$  criteria and default  $\alpha = 0.4, \lambda = 1$ ), whether adjusting the encoder weights  $\lambda = 2^{-k}$  in (b) or the transparency of the watermark in (c), is stronger.

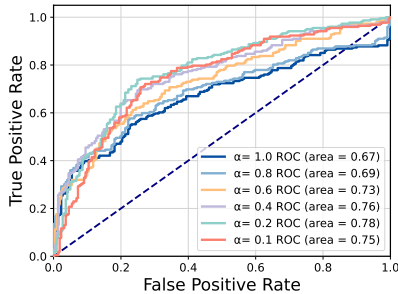
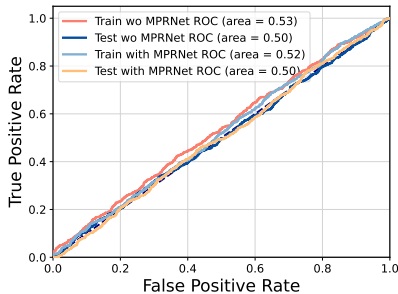


Figure 7: Result of image watermarks with reconstruction using MPRNet, measured by pixel distance.



(a) without Reconstruction

Figure 8: Results of a binary classification model for watermarks with and without MPRNet reconstruction.

viewing patterns of images, where the lower right area often receives less immediate attention.

**Extraction through Direct Pixel-wise Comparison.** Extraction results are illustrated in Figure 6a. Upon comparison using ROC curves and AUC values, we observe that image watermarks significantly underperform text watermarks in

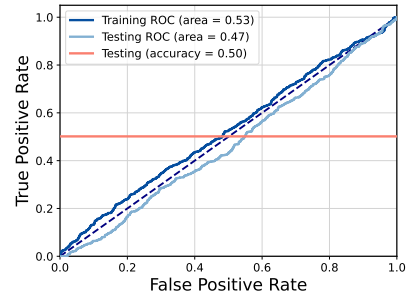


Figure 9: Invisibility test. The binary classification model fails to extract sufficient watermark information from images with invisible watermarks, making it unable to differentiate them from images without any watermark.

Figure 6b and Figure 6c (to be discussed in Subsection 6.3). For instance, when the transparency of the image watermark is set to 1, the AUC remains at a modest 0.58, which is substantially lower than the 0.85 AUC achieved by text watermarks with a transparency setting of 0.3. A plausible explanation for this discrepancy might be the greater challenge inherent in optimizing image watermarks.

**Extraction with Reconstruction.** To enhance the accuracy of watermark detection through pixel measurement, we explored using MPRNet for image watermark reconstruction. For this, we extracted the watermark portions from 1,000 watermarked images that had undergone editing, with each portion sized  $32 \times 32 \times 3$ . Additionally, we used their corresponding CIFAR-10 images as the targets for model training.

As shown in Figure 7, reconstruction helps recognition. Note that there is a caveat that we take the larger pixel-wise distance, which is supposed to be a negative case (not watermarked), as the positive (watermarked) case: On average, before reconstruction, the average distance between water-

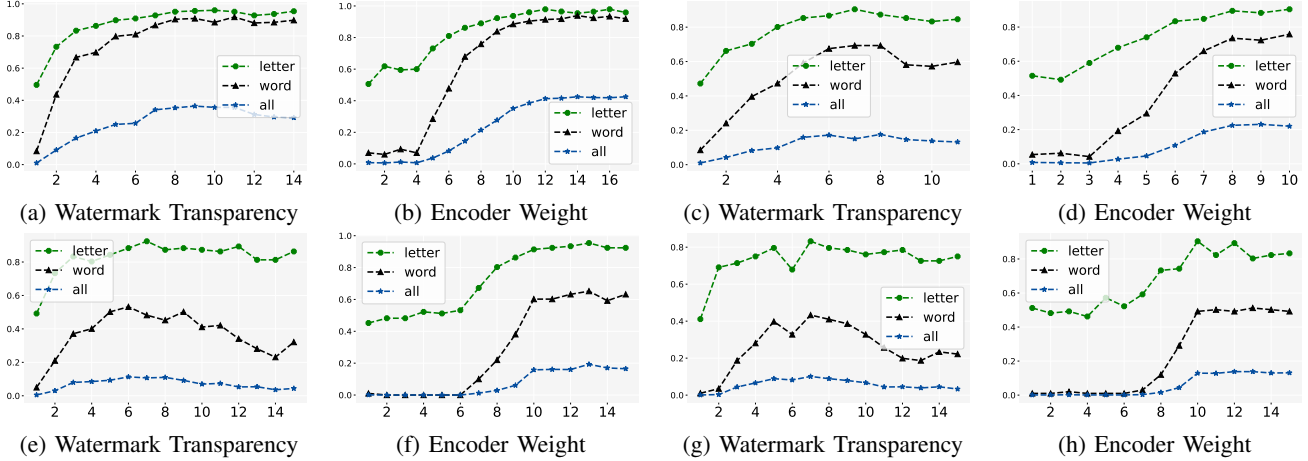


Figure 10: Watermark identification accuracy varies with the increase in watermark transparency and encoder weight on the LAION-Aesthetics (above) and TEDBench (below) datasets. Subfigures (a), (b), (e) and (f) display the outcomes when edited using the Instructpix2pix model, while (c), (d), (g) and (h) showcase results from editing via the Imagic model.

marked parts and the original CIFAR images is 147.9. However, after reconstruction, this distance increases to 162.2. Meanwhile, the average distance between non-watermarked parts and the original CIFAR images is 152.6. As a result, while the results shown in Figure 7 are promising, we cannot rely on them to detect watermarks.

We believe the issue comes from the characteristics of MPRNet in image post-processing. Since the pixel measurement method is highly *sensitive* to noise, the distance between the watermarked image and the watermark paradoxically increased after applying MPRNet. As shown in examples later in Figure 14 in Appendix B, image watermarks, due to the unique distribution of pixels in pictures, are completely obliterated post-editing, rendering them unrecognizable. However, for text watermarks, there is still evidence to be preserved after being edited.

**Extraction through a Binary Classifier.** To mitigate the negative impact of pixel distance, we further trained a binary classification model, under no MPRNet reconstruction, to discern whether image watermarks remain recognizable after editing. We collected 2,000 images, each watermarked and edited, then extracted a  $32 \times 32 \times 3$  section of the watermark from the edited images, labeling these as 1. Similarly, we extracted watermark sections from the edited originals, labeling these as 0. Moreover, the transparency  $\alpha$  of watermarks on these 2,000 images was randomly sampled between 0.1 and 1.0 to enhance the model’s generalization capability. However, as shown in Figure 8, we found that the model trained in this manner still failed to successfully identify image watermarks, as evidenced by an overall recognition accuracy of 0.5, equivalent to random guessing. Subsequently, we attempted to use the MPRNet reconstruction technique, only to find that it still failed to identify the image watermark, as reflected by a model accuracy of around 0.5.

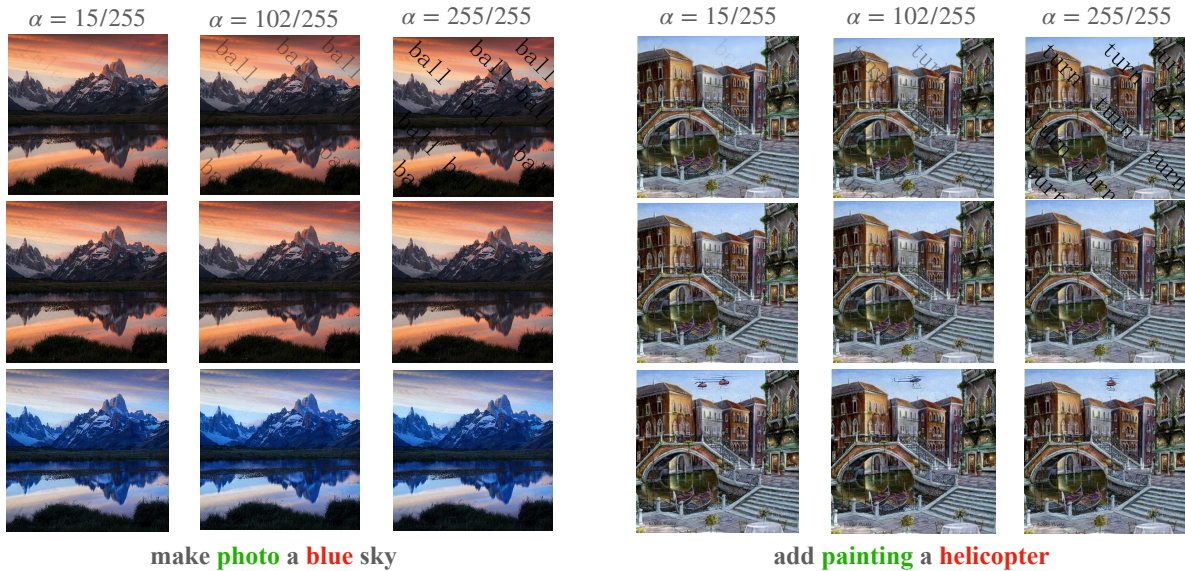
### 6.3. Results of Text Watermarks

**Invisibility.** To assert the invisibility of our watermark, we attempted to discern whether images had been embedded with an invisible watermark using a trained binary classification model. Specifically, we trained the model using 1,000 images from LAION-Aesthetics that had been watermarked (with randomly selected watermark transparency level  $\alpha$  from  $[0.2, 0.4, 0.6, 0.8, 1.0]$  for generalization) and subsequently edited by Instructpix2pix (i.e.,  $\hat{x}$  and  $\hat{x}_e$ ), along with their corresponding original images post-edit (i.e.,  $x$  and  $x_e$ ), labelled as 1 (watermarked) and 0 (not watermarked) respectively. The test set consisted of an additional 1,000 images. Despite various parameter tuning and model structural changes, the model could not distinguish between watermarked and non-watermarked images. This has been reflected in the test set inference results, as shown in Figure 9, yielding an accuracy of 0.501 and an AUC of 0.47.

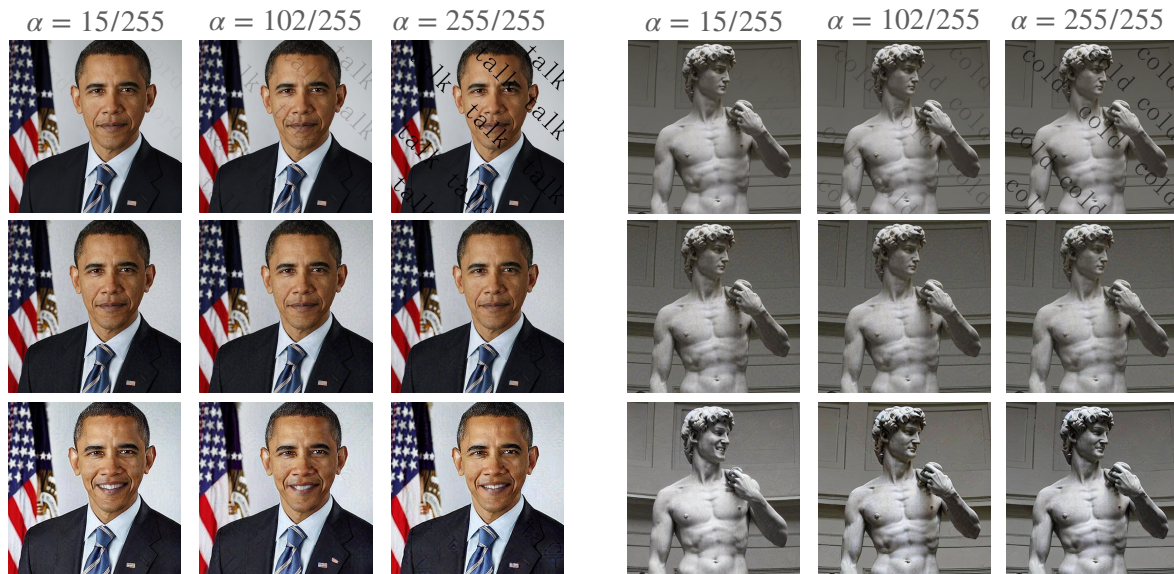
**Evaluation Metrics.** We first establish special accuracy function  $A$  for every text watermark region  $\hat{x}_k$  ( $k \in K$ ) with function Ext as follows,

$$A(\hat{x}_k) = \begin{cases} 1 & \text{if Ext}(\hat{x}_k) = w \\ 0 & \text{otherwise} \end{cases}$$

Similarly, we define  $A(\hat{x}_{n,k})$  as the  $k$ -th watermark in the  $n$ -th image. To quantify the watermark identification success in different scenarios, we define three metrics based on  $A$ : (1) First, we calculate the extraction accuracy rate of sub-watermarks across the entire test set as  $D_{\text{all}} = \frac{1}{NK} \sum_{n=1}^N \sum_{k=1}^K A(\hat{x}_{n,k})$ . (2) To measure the success rate of image ownership claims, we define metric  $D_{\text{word}} = \frac{1}{N} \sum_{n=1}^N \min \left\{ \sum_{k=1}^K A(\hat{x}_{n,k}), 1 \right\}$ . The implication of this metric is that among the  $K$  identical indepen-



(a) Examples of the Instructpix2pix model.



(b) Examples of the Imagic model.

Figure 11: In both subfigures, the first row represents the target images, denoted as  $x'$ , exhibiting varying watermark transparency  $\alpha$ . The second row displays the images after the watermark is injected, denoted as  $\hat{x}$ . The last row illustrates the corresponding edited images, denoted as  $\hat{x}_e$ .

dent watermarks we introduce, if even one is successfully recognized, it is deemed as proof of ownership. (3) Finally, we introduce metric  $D_{\text{letter}}$  to measure the identification success rate of special character watermarks. This method allows developers to use unique symbols as watermarks to stake their ownership claims. For instance, in an individual watermark containing  $M$  characters, only all  $M$  symbols are successfully identified within an image, and can be combined into the entire added symbol sequence, we consider

the watermark recognition to be successful.

As elaborated in [Subsection 4.2](#), our text watermark's strength in target images affects its visibility in edited images. The watermark's transparency and the weight of the encoder loss in our adversarial training both impact post-editing watermark extraction. Hence, we assess the impact of varying watermark transparency and encoder loss weights on extraction accuracy in the two editing models. Note that we ignore the false positives as we observe low average

false positive rates of 0%, 0%, and 25.5% on various  $\alpha$ , in LAION-Aesthetics dataset, across the three metrics for the no-watermark cases. In addition, to comprehensively assess the validity of our Ext, we calculated the ROC curves for Instructpix2pix under the  $D_{\text{letter}}$  mode across different values of  $\lambda$  and  $\alpha$ . The results are displayed in Figure 6b and Figure 6c. When  $\lambda = 1/8$  and  $\alpha = 0.3$ , the AUC values reach 0.93 and 0.85 respectively, indicating a certain degree of stability in the method.

**Results on LAION-Aesthetics.** Firstly, we evaluate the performance of our RIW on the LAION-Aesthetics dataset. As shown in Figure 10a and Figure 10c, we observed that as the transparency of the watermark in the target image  $x'$  increases, the extraction accuracy correspondingly improves across both Instructpix2pix and Imagic editing model. Moreover, it was found that beyond a certain level of transparency, specifically at around 102/255, the extraction accuracy across Instructpix2pix and Imagic begin to stabilize at 96.0% and 90.4%, respectively. As evident from Figure 11a, when the transparency reaches 102/255, the watermark we injected becomes visually imperceptible in the edited images. Meanwhile, even when the transparency is as low as 15/255, the watermark can still be successfully extracted. Similar results were observed with adjustments to the encoder weight  $\lambda$ . As illustrated in Figure 10b and Figure 10d, when we increase  $\lambda$  to 1/2 or lower, our  $D_{\text{letter}}$  success rate stabilizes at 97.9% and 90.4%.

**Results on TEdBench.** Similar results are observed on the TEdBench dataset with both two editing models, as shown in Figure 10e and Figure 10g. Once the watermark transparency for  $x'$  reaches 51/255, watermark identification accuracy levels off. In both the Instructpix2pix and Imagic models, when the watermark transparency is 51/255, the identification accuracy reaches respective accuracies of 92.4% and 83.2%. Additionally, as shown Figure 10f and Figure 10h, when  $\lambda$  is below 1/2, identification accuracy progressively becomes stable, attaining values of 91.4% and 89.3% respectively when  $\lambda$  is equal to 1/2. The TEdBench dataset, with 50 images and 100 editing instructions, is inadequate for training Ext, which was trained exclusively on LAION-Aesthetics. This contributes to the observed lower watermark identification accuracy on TEdBench. A dip in accuracy occurs, as seen in Figure 10g, when watermark transparency surpasses 102/255, likely due to Ext’s training with watermarks in  $x'$  at this default transparency. Still, Ext demonstrates satisfactory generalizability, with Imagic editing results in Figure 11b.

**Impact of Encoder Weight.** We evaluate the impact of changes in the weight of encoder loss on the invisibility of watermarks after being edited. As  $\lambda$  approaches 1/2, the watermark extraction accuracy stabilizes, as shown in Figure 10. However, when  $\lambda$  reaches 1/128, we can faintly discern a subtle watermark after editing. As examples shown in Figure 15 in Appendix B, users can adjust the watermark strength parameter in our optimization function to determine

TABLE 3: Improvement in watermark identification accuracy for both editing models Instructpix2pix (Ipx), Imagic (Igc) and datasets LAION-Aesthetics (LA), TEdBench (TB) under conditions of low watermark clarity when introducing reconstruction. Specifically, these results are obtained when transparency  $\alpha$  is set to 1/255 and  $\lambda$  is  $5e10$ . Both of them control watermark strength (Stren). In the table, “w/o Rec” denotes results without reconstruction, while “w/ Rec” indicates results with reconstruction.  $\Delta$  indicates improvement of the reconstruction.

Edit	Dataset	Stren	w/o Rec	w/ Rec	$\Delta$
Ipx	LA	$\alpha$	49.6%	54.3%	<b>9.5%</b>
		$\lambda$	50.6%	55.7%	<b>10.1%</b>
	TB	$\alpha$	49.2%	49.2%	0%
		$\lambda$	45.2%	45.2%	0%
Igc	LA	$\alpha$	47.2%	50.7%	<b>7.4%</b>
		$\lambda$	51.5%	57.0%	<b>10.7%</b>
	TB	$\alpha$	41.1%	42.1%	<b>2.4%</b>
		$\lambda$	51.2%	52.2%	<b>2.0%</b>

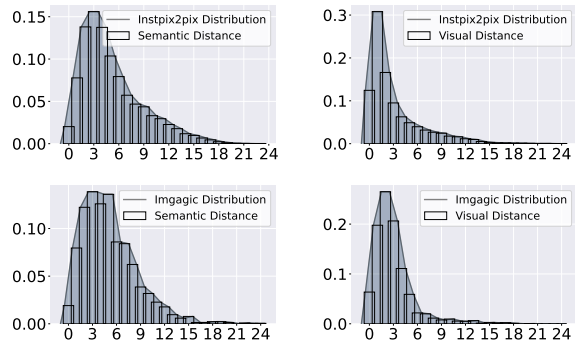


Figure 12: Distribution of semantic and visual changes before and after editing with the Instructpix2pix and Imagic models. The first row shows the distribution for the Instructpix2pix model with semantic and vision distance (very close), while the second row shows those for the Imagic model.

the visibility of the watermark after the image is edited. When the watermark is conspicuous, it serves as a warning against malicious edits. When the watermark is invisible, it assists in claiming the copyright of the edited image.

#### 6.4. Benefit of Reconstruction

We evaluate the efficacy of the reconstruction component in our method. We observe that under conditions where watermark clarity is extremely low, the reconstruction can be beneficial. For instance, on the LAION-Aesthetics dataset using the Instructpix2pix, when watermark transparency is set to 1/255 or  $\lambda$  is set to  $5e4$ , there is an increase in identification accuracy by 9.5% and 10.1%, respectively. For a more comprehensive view of results across two edit models and two datasets of low clarity watermark shown in Table 3. When the extraction accuracy of text

TABLE 4: Watermark extraction accuracy for the top 5% based on the Semantic (Sem) and Vision (Vis) distance (Dist) before and after editing with `Instructpix2pix` (Ipx) and `Imagic` (Igc) respectively, along with the specific distance threshold (Thred).

Edit	Dist	Thred	$D_{\text{letter}}\downarrow$	$D_{\text{word}}\downarrow$	$D_{\text{all}}\downarrow$
Ipx	Sem	0.44	0.21%	0.51%	2.73%
	Vis	0.62	0.23%	0.56%	3.27%
Igc	Sem	0.30	0.06%	0.11%	0.07%
	Vis	0.42	0.11%	0.32%	0.00%

watermarks is already high, the improvement brought about by reconstruction techniques is not significant. Furthermore, watermark reconstruction technology is more effective for text watermarks than for image watermarks, reflecting certain limitations of the reconstruction model MPRNet [61].

## 6.5. Watermark Protection Boundary

Considering that editing models can modify an image’s distribution and semantics, preserving ownership amid significant changes to the image’s content or style becomes crucial. Thus, we assess the degree of alteration in the image’s semantic or visual content after editing with either the `Imagic` or `Instructpix2pix` models. As the distance in both semantic and visual dimensions increases, the watermark becomes increasingly difficult to extract due to the loss of original image information. Figure 12 displays the distribution of changes in images before and after editing. The two images on the left represent the semantic distance based on CLIP [39], while the two images on the right show the visual distance calculated using VGG [50]. Specifically, akin to existing works [39], [65], [46], when calculating distances using CLIP and VGG, we first project the images onto embeddings and then compute the  $\ell_2$  distance between these embeddings.

As observed from Table 4, when we incorporate the top 5% of images with the largest changes in semantic and vision distance into our analysis, there is a varying degree of decline in the accuracy of different watermark extraction strategies. Notably, the `Instructpix2pix` model tends to have a more significant impact than the `Imagic`. This is attributed to the fact that `Instructpix2pix` induces a larger shift in the image distribution, as also indicated by the distance threshold (Thred), i.e., 46.7% and 47.5% higher in semantic and vision distance than `Imagic`. The overall accuracy of text watermark extraction, as it varies with the edit distance, is illustrated by Figure 16 in Appendix B.

As illustrated in Figure 13, a detailed comparison of the visual changes between the original and edited images, based on the two different models, reveals a notable observation. When the distance between the original and edited versions is substantial, the alterations in the images are quite significant. This leads to the edited images retaining minimal resemblance to their original counterparts. Consequently,

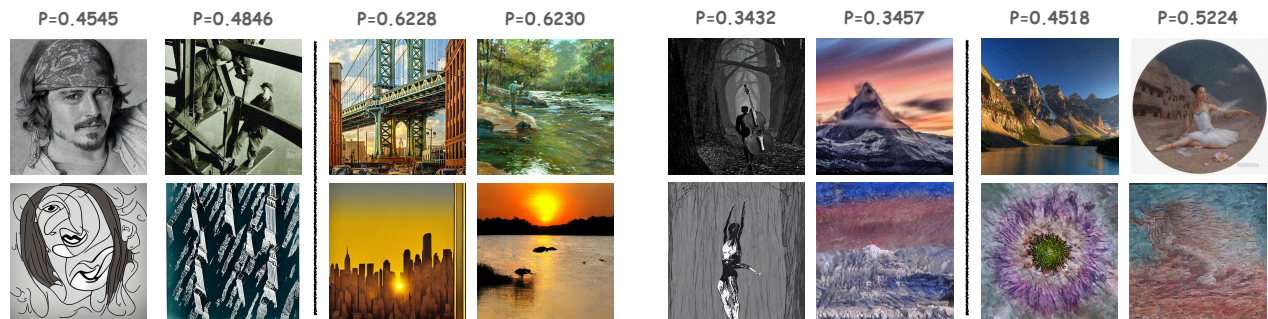
such extensive modifications raise a question about the necessity of further discussions regarding copyright protection. The stark contrast in visual appearance suggests that the edited images might be viewed as distinct enough to mitigate concerns over copyright infringement.

## 7. Conclusion

In this paper, we are the first to address the issue of image copyright and malicious alterations within the context of diffusion model-based editing frameworks. We have formalized this issue and presented it within a Game framework. Subsequently, we conduct an exhaustive study of prior watermarking techniques, such as digital watermarks or AutoEncoder-based watermarks. We discover that traditional watermarking approaches, even when enhanced, are inadequate to handle the challenges introduced by the editing models of the diffusion era. Building on this, we propose our invisible watermarking method RIW (Robust Invisible Watermarking) based on visual-semantic information. Compared to traditional watermarking techniques with 0% retention, our method maintains a 96.0% watermark extraction accuracy post-editing. This ensures that our watermark effectively addresses the image copyright and deceptive editing concerns in the editing model framework.

## References

- [1] Rameen Abdal, Yipeng Qin, and Peter Wonka. Image2stylegan: How to embed images into the stylegan latent space? In *Proceedings of the IEEE/CVF international conference on computer vision*, pages 4432–4441, 2019.
- [2] Rameen Abdal, Yipeng Qin, and Peter Wonka. Image2stylegan++: How to edit the embedded images? In *Proceedings of the IEEE/CVF conference on computer vision and pattern recognition*, pages 8296–8305, 2020.
- [3] Robin Rombach Aleksander Holynski. `instruct-pix2pix`. <https://github.com/timothybrooks/instruct-pix2pix>, 2023.
- [4] Omri Avrahami, Dani Lischinski, and Ohad Fried. Blended diffusion for text-driven editing of natural images. In *Proceedings of the IEEE/CVF Conference on Computer Vision and Pattern Recognition*, pages 18208–18218, 2022.
- [5] Yogesh Balaji, Seungjun Nah, Xun Huang, Arash Vahdat, Jiaming Song, Karsten Kreis, Miika Aittala, Timo Aila, Samuli Laine, Bryan Catanzaro, et al. ediffi: Text-to-image diffusion models with an ensemble of expert denoisers. *arXiv preprint arXiv:2211.01324*, 2022.
- [6] Andreas Blattmann, Robin Rombach, Huan Ling, Tim Dockhorn, Seung Wook Kim, Sanja Fidler, and Karsten Kreis. Align your latents: High-resolution video synthesis with latent diffusion models. In *Proceedings of the IEEE/CVF Conference on Computer Vision and Pattern Recognition*, pages 22563–22575, 2023.
- [7] Tim Brooks, Aleksander Holynski, and Alexei A Efros. `Instruct-pix2pix`: Learning to follow image editing instructions. In *Proceedings of the IEEE/CVF Conference on Computer Vision and Pattern Recognition*, pages 18392–18402, 2023.
- [8] Tom Brown, Benjamin Mann, Nick Ryder, Melanie Subbiah, Jared D Kaplan, Prafulla Dhariwal, Arvind Neelakantan, Pranav Shyam, Girish Sastry, Amanda Askell, et al. Language models are few-shot learners. *Advances in neural information processing systems*, 33:1877–1901, 2020.



(a) Examples edited by Instructpix2pix

(b) Examples edited by Imagic

Figure 13: Examples with notable semantic and vision distances before (first row) and after (second row) editing by the Instructpix2pix and Imagic edit models. In each subfigure, the left panel represents semantic distance while the right shows vision distance. P indicates the corresponding distance values.

- [9] Ruoxi Chen, Haibo Jin, Jinyin Chen, and Lichao Sun. Editshield: Protecting unauthorized image editing by instruction-guided diffusion models. *arXiv preprint arXiv:2311.12066*, 2023.
- [10] Ingemar Cox, Matthew Miller, Jeffrey Bloom, and Chris Honsinger. Digital watermarking. *Journal of Electronic Imaging*, 11(3):414–414, 2002.
- [11] Yingqian Cui, Jie Ren, Han Xu, Pengfei He, Hui Liu, Lichao Sun, and Jiliang Tang. Diffusionshield: A watermark for copyright protection against generative diffusion models. *arXiv preprint arXiv:2306.04642*, 2023.
- [12] Prafulla Dhariwal and Alexander Nichol. Diffusion models beat gans on image synthesis. *Advances in neural information processing systems*, 34:8780–8794, 2021.
- [13] Krizhevsky et al. CIFAR-10 and CIFAR-100 dataset and analysis. . <https://www.cs.toronto.edu/~kriz/cifar.html>, 2013. [Online; accessed 15-March-2022].
- [14] Ian Goodfellow, Jean Pouget-Abadie, Mehdi Mirza, Bing Xu, David Warde-Farley, Sherjil Ozair, Aaron Courville, and Yoshua Bengio. Generative adversarial nets. *Advances in neural information processing systems*, 27, 2014.
- [15] Ian J Goodfellow, Jonathon Shlens, and Christian Szegedy. Explaining and harnessing adversarial examples. *arXiv preprint arXiv:1412.6572*, 2014.
- [16] Tianyu Gu, Brendan Dolan-Gavitt, and Siddharth Garg. Badnets: Identifying vulnerabilities in the machine learning model supply chain. *arXiv preprint arXiv:1708.06733*, 2017.
- [17] Amir Hertz, Ron Mokady, Jay Tenenbaum, Kfir Aberman, Yael Pritch, and Daniel Cohen-Or. Prompt-to-prompt image editing with cross attention control. *arXiv preprint arXiv:2208.01626*, 2022.
- [18] Jonathan Ho, Ajay Jain, and Pieter Abbeel. Denoising diffusion probabilistic models. *Advances in neural information processing systems*, 33:6840–6851, 2020.
- [19] Jonathan Ho, Chitwan Saharia, William Chan, David J Fleet, Mohammad Norouzi, and Tim Salimans. Cascaded diffusion models for high fidelity image generation. *The Journal of Machine Learning Research*, 23(1):2249–2281, 2022.
- [20] Jonathan Ho and Tim Salimans. Classifier-free diffusion guidance. *arXiv preprint arXiv:2207.12598*, 2022.
- [21] Xun Huang, Ming-Yu Liu, Serge Belongie, and Jan Kautz. Multimodal unsupervised image-to-image translation. In *Proceedings of the European conference on computer vision (ECCV)*, pages 172–189, 2018.
- [22] Phillip Isola, Jun-Yan Zhu, Tinghui Zhou, and Alexei A Efros. Image-to-image translation with conditional adversarial networks. In *Proceedings of the IEEE conference on computer vision and pattern recognition*, pages 1125–1134, 2017.
- [23] Zhengyuan Jiang, Jinghui Zhang, and Neil Zhenqiang Gong. Evading watermark based detection of ai-generated content. *arXiv preprint arXiv:2305.03807*, 2023.
- [24] Tero Karras, Samuli Laine, and Timo Aila. A style-based generator architecture for generative adversarial networks. In *Proceedings of the IEEE/CVF conference on computer vision and pattern recognition*, pages 4401–4410, 2019.
- [25] Tero Karras, Samuli Laine, and Timo Aila. A style-based generator architecture for generative adversarial networks. In *Proceedings of the IEEE/CVF conference on computer vision and pattern recognition*, pages 4401–4410, 2019.
- [26] Bahjat Kawar, Shiran Zada, Oran Lang, Omer Tov, Huiwen Chang, Tali Dekel, Inbar Mosseri, and Michal Irani. Imagic: Text-based real image editing with diffusion models. In *Proceedings of the IEEE/CVF Conference on Computer Vision and Pattern Recognition*, pages 6007–6017, 2023.
- [27] Zhifeng Kong, Wei Ping, Jiayi Huang, Kexin Zhao, and Bryan Catanzaro. Diffwave: A versatile diffusion model for audio synthesis. *arXiv preprint arXiv:2009.09761*, 2020.
- [28] Chumeng Liang and Xiaoyu Wu. Mist: Towards improved adversarial examples for diffusion models, 2023.
- [29] Chumeng Liang, Xiaoyu Wu, Yang Hua, Jiaru Zhang, Yiming Xue, Tao Song, XUE Zhengui, Ruhui Ma, and Haibing Guan. Adversarial example does good: Preventing painting imitation from diffusion models via adversarial examples. 2023.
- [30] Ming-Yu Liu, Xun Huang, Arun Mallya, Tero Karras, Timo Aila, Jaakko Lehtinen, and Jan Kautz. Few-shot unsupervised image-to-image translation. In *Proceedings of the IEEE/CVF international conference on computer vision*, pages 10551–10560, 2019.
- [31] Yugeng Liu, Zheng Li, Michael Backes, Yun Shen, and Yang Zhang. Watermarking diffusion model. *arXiv preprint arXiv:2305.12502*, 2023.
- [32] Nils Lukas, Abdulrahman Diaa, Lucas Fenaux, and Florian Kerschbaum. Leveraging optimization for adaptive attacks on image watermarks. *arXiv preprint arXiv:2309.16952*, 2023.
- [33] Nils Lukas and Florian Kerschbaum. Ptw: Pivotal tuning watermarking for pre-trained image generators. *arXiv preprint arXiv:2304.07361*, 2023.
- [34] Aleksander Madry, Aleksandar Makelov, Ludwig Schmidt, Dimitris Tsipras, and Adrian Vladu. Towards deep learning models resistant to adversarial attacks. *arXiv preprint arXiv:1706.06083*, 2017.
- [35] Chenlin Meng, Yutong He, Yang Song, Jiaming Song, Jiajun Wu, Jun-Yan Zhu, and Stefano Ermon. Sdedit: Guided image synthesis and editing with stochastic differential equations. *arXiv preprint arXiv:2108.01073*, 2021.

- [36] Alex Nichol, Prafulla Dhariwal, Aditya Ramesh, Pranav Shyam, Pamela Mishkin, Bob McGrew, Ilya Sutskever, and Mark Chen. Glide: Towards photorealistic image generation and editing with text-guided diffusion models. *arXiv preprint arXiv:2112.10741*, 2021.
- [37] Sen Peng, Yufei Chen, Cong Wang, and Xiaohua Jia. Protecting the intellectual property of diffusion models by the watermark diffusion process. *arXiv preprint arXiv:2306.03436*, 2023.
- [38] Ben Poole, Ajay Jain, Jonathan T Barron, and Ben Mildenhall. Dreamfusion: Text-to-3d using 2d diffusion. *arXiv preprint arXiv:2209.14988*, 2022.
- [39] Alec Radford, Jong Wook Kim, Chris Hallacy, Aditya Ramesh, Gabriel Goh, Sandhini Agarwal, Girish Sastry, Amanda Askell, Pamela Mishkin, Jack Clark, et al. Learning transferable visual models from natural language supervision. In *International conference on machine learning*, pages 8748–8763. PMLR, 2021.
- [40] Aditya Ramesh, Prafulla Dhariwal, Alex Nichol, Casey Chu, and Mark Chen. Hierarchical text-conditional image generation with clip latents, 2022. URL <https://arxiv.org/abs/2204.06125>, 7, 2022.
- [41] Aditya Ramesh, Mikhail Pavlov, Gabriel Goh, Scott Gray, Chelsea Voss, Alec Radford, Mark Chen, and Ilya Sutskever. Zero-shot text-to-image generation. In *International Conference on Machine Learning*, pages 8821–8831. PMLR, 2021.
- [42] Robin Rombach, Andreas Blattmann, Dominik Lorenz, Patrick Esser, and Björn Ommer. High-resolution image synthesis with latent diffusion models. In *Proceedings of the IEEE/CVF conference on computer vision and pattern recognition*, pages 10684–10695, 2022.
- [43] Nataniel Ruiz, Yuanzhen Li, Varun Jampani, Yael Pritch, Michael Rubinstein, and Kfir Aberman. Dreambooth: Fine tuning text-to-image diffusion models for subject-driven generation. In *Proceedings of the IEEE/CVF Conference on Computer Vision and Pattern Recognition*, pages 22500–22510, 2023.
- [44] Chitwan Saharia, William Chan, Saurabh Saxena, Lala Li, Jay Whang, Emily L Denton, Kamyar Ghasemipour, Raphael Gontijo Lopes, Burcu Karagol Ayan, Tim Salimans, et al. Photorealistic text-to-image diffusion models with deep language understanding. *Advances in Neural Information Processing Systems*, 35:36479–36494, 2022.
- [45] Chitwan Saharia, Jonathan Ho, William Chan, Tim Salimans, David J Fleet, and Mohammad Norouzi. Image super-resolution via iterative refinement. *IEEE Transactions on Pattern Analysis and Machine Intelligence*, 45(4):4713–4726, 2022.
- [46] Florian Schroff, Dmitry Kalenichenko, and James Philbin. Facenet: A unified embedding for face recognition and clustering. In *Proceedings of the IEEE conference on computer vision and pattern recognition*, pages 815–823, 2015.
- [47] Christoph Schuhmann, Romain Beaumont, Richard Vencu, Cade Gordon, Ross Wightman, Mehdi Cherti, Theo Coombes, Aarush Katta, Clayton Mullis, Mitchell Wortsman, et al. Laion-5b: An open large-scale dataset for training next generation image-text models. *Advances in Neural Information Processing Systems*, 35:25278–25294, 2022.
- [48] Shawn Shan, Jenna Cryan, Emily Wenger, Haitao Zheng, Rana Hanocka, and Ben Y Zhao. Glaze: Protecting artists from style mimicry by text-to-image models. *arXiv preprint arXiv:2302.04222*, 2023.
- [49] Frank Y Shih and Scott YT Wu. Combinational image watermarking in the spatial and frequency domains. *Pattern Recognition*, 36(4):969–975, 2003.
- [50] Karen Simonyan and Andrew Zisserman. Very deep convolutional networks for large-scale image recognition. *arXiv preprint arXiv:1409.1556*, 2014.
- [51] Uriel Singer, Adam Polyak, Thomas Hayes, Xi Yin, Jie An, Songyang Zhang, Qiyuan Hu, Harry Yang, Oron Ashual, Oran Gafni, et al. Make-a-video: Text-to-video generation without text-video data. *arXiv preprint arXiv:2209.14792*, 2022.
- [52] Jascha Sohl-Dickstein, Eric Weiss, Niru Maheswaranathan, and Surya Ganguli. Deep unsupervised learning using nonequilibrium thermodynamics. In *International conference on machine learning*, pages 2256–2265. PMLR, 2015.
- [53] Jiaming Song, Chenlin Meng, and Stefano Ermon. Denoising diffusion implicit models. *arXiv preprint arXiv:2010.02502*, 2020.
- [54] Yang Song and Stefano Ermon. Generative modeling by estimating gradients of the data distribution. *Advances in neural information processing systems*, 32, 2019.
- [55] Yang Song, Jascha Sohl-Dickstein, Diederik P Kingma, Abhishek Kumar, Stefano Ermon, and Ben Poole. Score-based generative modeling through stochastic differential equations. *arXiv preprint arXiv:2011.13456*, 2020.
- [56] Xuan Su, Jiaming Song, Chenlin Meng, and Stefano Ermon. Dual diffusion implicit bridges for image-to-image translation. *arXiv preprint arXiv:2203.08382*, 2022.
- [57] Pascal Vincent. A connection between score matching and denoising autoencoders. *Neural computation*, 23(7):1661–1674, 2011.
- [58] Yuxin Wen, John Kirchenbauer, Jonas Geiping, and Tom Goldstein. Tree-ring watermarks: Fingerprints for diffusion images that are invisible and robust. *arXiv preprint arXiv:2305.20030*, 2023.
- [59] Mengjiao Yang, Yilun Du, Bo Dai, Dale Schuurmans, Joshua B Tenenbaum, and Pieter Abbeel. Probabilistic adaptation of text-to-video models. *arXiv preprint arXiv:2306.01872*, 2023.
- [60] Ning Yu, Vladislav Skripniuk, Sahar Abdelnabi, and Mario Fritz. Artificial fingerprinting for generative models: Rooting deepfake attribution in training data. In *Proceedings of the IEEE/CVF International conference on computer vision*, pages 14448–14457, 2021.
- [61] Syed Waqas Zamir, Aditya Arora, Salman Khan, Munawar Hayat, Fahad Shahbaz Khan, Ming-Hsuan Yang, and Ling Shao. Multi-stage progressive image restoration. In *Proceedings of the IEEE/CVF conference on computer vision and pattern recognition*, pages 14821–14831, 2021.
- [62] Brian Hu Zhang, Blake Lemoine, and Margaret Mitchell. Mitigating unwanted biases with adversarial learning. In *Proceedings of the 2018 AAAI/ACM Conference on AI, Ethics, and Society*, pages 335–340, 2018.
- [63] Hongyi Zhang, Moustapha Cisse, Yann N Dauphin, and David Lopez-Paz. mixup: Beyond empirical risk minimization. *arXiv preprint arXiv:1710.09412*, 2017.
- [64] Kevin Alex Zhang, Lei Xu, Alfredo Cuesta-Infante, and Kalyan Veeramachaneni. Robust invisible video watermarking with attention. *arXiv preprint arXiv:1909.01285*, 2019.
- [65] Richard Zhang, Phillip Isola, Alexei A Efros, Eli Shechtman, and Oliver Wang. The unreasonable effectiveness of deep features as a perceptual metric. In *Proceedings of the IEEE conference on computer vision and pattern recognition*, pages 586–595, 2018.
- [66] Xuandong Zhao, Kexun Zhang, Zihao Su, Saastha Vasani, Ilya Grishchenko, Christopher Kruegel, Giovanni Vigna, Yu-Xiang Wang, and Lei Li. Invisible image watermarks are provably removable using generative ai, 2023.
- [67] Yunqing Zhao, Tianyu Pang, Chao Du, Xiao Yang, Ngai-Man Cheung, and Min Lin. A recipe for watermarking diffusion models. *arXiv preprint arXiv:2303.10137*, 2023.

## Appendix A. Additional Background

We first present Denoising Diffusion Probabilistic Models (DDPMs) [18], which serve as the foundation for image editing models, and then, we dive into detailed descriptions of two state-of-the-art and open-sourced edit models we use in this paper.

## A.1. Denoising Diffusion Probabilistic Models

In DDPMs, a data item  $x_0$ , sampling from the original distribution, undergoes a forward diffusion process to gradually approach the Gaussian distribution  $N(0, 1)$ . The reverse diffusion starts with a noise image sampled from  $x_T \sim N(0, 1)$  and progressively refines it into a photorealistic image  $x_0$ . Each intermediate sample,  $x_t$ , for  $t \in 1, \dots, T$ , adheres to the format,

$$x_t = \sqrt{a_t}x_0 + \sqrt{1 - a_t}\varepsilon_t$$

with the hyper-parameter  $a_t \in (0, 1)$  of the diffusion schedule and  $\varepsilon_t \sim N(0, I)$ , each refinement step is predicted using the neural network model  $f_\theta$ . Therefore,  $x_{t-1}$  is derived from  $f_\theta(x_t, t)$ , followed by a Gaussian perturbation as,

$$x_{t-1} = f_\theta(x_t, t) + \sigma_t z$$

with  $z \sim N(0, I)$ . The training objective of  $f_\theta$  is optimized by variational lower bound as [18], [52],

$$L_t = \mathbb{E}_{t \sim [1, T], x_0, \varepsilon_t} \left[ \left\| \varepsilon_t - f_\theta(\sqrt{a_t}x_0 + \sqrt{1 - a_t}\varepsilon_t, t) \right\|_2^2 \right]$$

DDPM can be adapted to learn conditional distributions by conditioning the denoising neural network  $f_\theta$  on an auxiliary input  $y$ . Consequently, the network  $f_\theta(x_t, t, y)$  samples from a data distribution based on  $y$ . Typically,  $y$  is a descriptive text for the training image [40], [5], [43], [44]. However,  $y$  can also represent a low-resolution image [45] or a class label in ImageNet [19]. For our editing tasks,  $y$  encompasses both the edited image and text prompt [7], [26].

## A.2. Details about Editing Models

**Instructpix2pix.** It utilizes a pre-trained Stable Diffusion (SD) [42] model as the base model. SD incorporates DDPM [18] for the diffusion process and CLIP [39] for semantic alignment with textual descriptions. The image inference process involves projecting images into the *latent space* using an encoder  $E$ , and then restoring them back to images with a corresponding decoder  $D$ . During the editing process, the target image for editing,  $x$ , and the editing instructions,  $p$ , are fed into SD. The edited image is then gradually inferred from random Gaussian noise  $z_t$ , with each step  $t$  of inference targeting to achieve the objective as follows,

$$L = \mathbb{E}_{E(x), p, \varepsilon \sim N(0, 1), t} \left[ \left\| \varepsilon_t - f_\theta(z_t, t, E(x), p) \right\|_2^2 \right]$$

where  $f_\theta$  represents a U-Net model tasked with predicting the noise  $\varepsilon_t$  at each step of the process. The authors gather pairs of images  $x$ , as shown in Figure 1, differing only as described by the text instruction  $p$ . Therefore, the U-Net model learns to produce corresponding edited images based on the input image and text prompt from Gaussian noise. Importantly, Instructpix2pix applies Classifier-free guidance [20], which makes the sampled images better

correspond with the conditioning. Additionally, it employs a linear combination strategy to balance the influence of conditional and unconditional factors during model training.

Here, we introduce the unique classifier-free guidance [20] design of Instructpix2pix [7]: To balance the effects of conditional and unconditional aspects during model training, the basic linear combination of the conditional and unconditional score estimates is designed as follows:

$$\tilde{f}_\theta(z_t, c) = (1 + s)f_\theta(z_t, c) - sf_\theta(z_t, \emptyset)$$

in typical score estimation functions,  $c$  is the condition, but in our editing task, there are two conditions, i.e., the original image  $x$  and the edit instruction  $p$ . The modified score estimate is as follows,

$$\begin{aligned} \tilde{f}_\theta(z_t, x, p) &= f_\theta(z_t, \emptyset, \emptyset) \\ &+ s_I \cdot [f_\theta(z_t, x, \emptyset) - f_\theta(z_t, \emptyset, \emptyset)] \\ &+ s_T \cdot [f_\theta(z_t, x, p) - f_\theta(z_t, x, \emptyset)] \end{aligned}$$

Where the guidance scales  $s_I$  and  $s_T$  are hyper-parameters that adjust the relevance between generated samples and the input image and edit instruction, respectively.

**Imagic.** It does not need pairs of images like Instructpix2pix, due to its unique fine-tuning paradigm. Their approach involves three steps. In the first step, it encodes the edit instruction with CLIP text [39] and optimizes the embedding, making it close to the input image in the latent space. In the second step, it fine-tunes the generative diffusion model, i.e., Stable Diffusion [42], with this embedding for improved image reconstruction. In the last step, it linearly interpolates the target and optimized text embeddings. This blended representation undergoes the diffusion process in their fine-tuned model, producing the final edited image. Additionally, Imagic freely integrates with various text-to-image diffusion models [26]. The researchers assessed their editing approach on both Imagen [44] and Stable Diffusion [42]. In our study, we employed the editing pipeline from version “sd-v1-4-full-ema.ckpt” of Stable Diffusion available on GitHub<sup>7</sup>, which is highly similar in structure and training data to the version “sd-v1.5.ckpt” used by Instructpix2pix.

**Text Edit Prompt.** Brooks et al. used 700 captions from the LAION-Aesthetics dataset [47], enhanced with manual editing instructions and output captions [7]. They fine-tuned a GPT-3 model [8] for automated instruction generation. We evaluate using this augmented LAION-Aesthetics dataset. However, different models have entirely different styles of edit instructions, as shown in Table 5. The edit instruction for Instructpix2pix starts with a verb, essentially functioning as a command, whereas the edit instruction for Imagic describes the image after the editing process to guide the model’s editing. Brooks et al. provide two styles of edit instructions based on the LAION-Aesthetics dataset [7].

7. <https://github.com/justinpinkney/stable-diffusion/blob/main/notebooks/imagix.ipynb>

TABLE 5: Different style of text edit instruction between `Instructpix2pix` (ipx) [7] and `Imagic` (igc) [26].

	Romantic Venice Oil Paintings		A photo of Barack Obama
Instruction Style	ipx	Add painting a helicopter	Turn Barack Obama into smiling with a big grin
	igc	Romantic Venice with Helicopter Oil Paintings	A photo of Barack Obama smiling with a big grin

TABLE 6: An automated dialogue to generate edit instructions based on GPT-4-0613 API, tailored to match the prompt styles of various editing models.

**Prompt:** Let’s play a game. I’ll provide a sentence A, which describes an image, for example: “the little prince fox wallpaper”. Then, I’ll give a modification instruction C for that image, such as “make the fox roguish”. The outcome will be a modified description, sentence B, which could be: “roguish fox wallpaper”. In our game, I’ll supply you with sentences A and B, and your task is to deduce the corresponding modification instruction, sentence C. Require C naturally like the image editing instruction.

**GPT4:** Sounds like an interesting challenge, let’s go for it!

**Prompt:** Now, I provide the sentence A “A photo of a standing dog” and sentence B “A photo of a sitting dog”. Now answer me with the corresponding instruction sentence C.

**GPT4:** Change the standing dog into a sitting position.

**Prompt:** Now, I provide the sentence A “A photo of a tennis ball” and sentence B “A photo of a tomato in a blue tennis court”. Now answer me with the corresponding instruction sentence C.

**GPT4:** Replace the tennis ball with a tomato in a blue tennis court.

.....

**Prompt:** Now, I provide sentence A “A photo of a teddy” and sentence B “A photo of a teddy bear doing pushups”. Now answer me with the corresponding instruction sentence C.

**GPT4:** Make the teddy bear look like it’s doing pushups.

However, the TedBench dataset has no corresponding edit instructions for the `Instructpix2pix` model. To address this, we generated the corresponding instruction styles using the GPT-4 API, as shown in Table 6. Compared to fine-tuning with GPT-3 and data collecting, which costs thousands of dollars [3], this approach costs 6.2 dollars while achieving identical results.

## Appendix B. Additional Results

Figure 14 displays two examples: one is a target image with an image watermark, and the other with a text watermark. We directly edit these two images using the `Instructpix2pix` model. The corresponding results of these edits show that watermarks using images often become difficult to discern after being edited by a diffusion model, blending more into the original image. In contrast, text watermarks can be preserved. This may also contribute to the easier extraction of text watermarks.

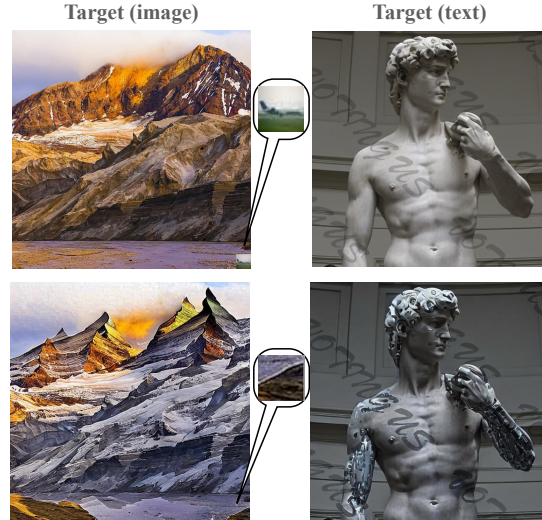
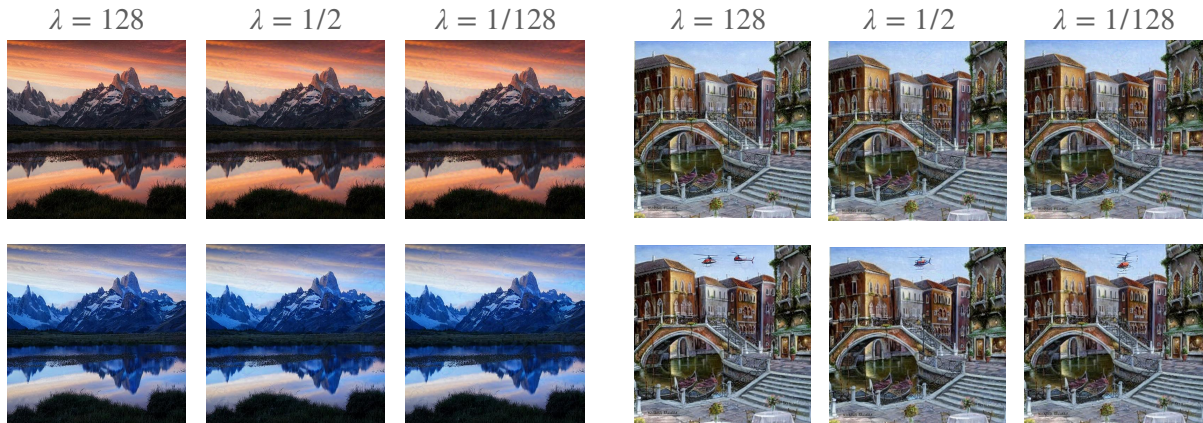


Figure 14: Examples showing some intuitions why image watermarks (left column) do not work while text watermarks (right column) do. The first row displays the target, which is a CIFAR10 image overlapped at the bottom right corner of the original image, and the text overlapped on an image. The second row shows the corresponding edited images. The image watermark in the bottom right image does not retain much information about the watermark after editing. In contrast, the text watermark remains clearly visible.

Figure 15 demonstrates the varying degrees of visibility of text watermarks under editing by the `Instructpix2pix` and `Imagic` models, throughout the optimization process, as encoder weight changes. For the `Instructpix2pix` model, the watermark remains inconspicuous at a higher weight value, i.e.,  $\lambda = 1/128$ . In contrast, with the `Imagic` model, the watermark in the edited images becomes progressively more distinct as  $\lambda$  reaches  $1/2$ .

Figure 16 illustrates the variation in accuracy of our three watermark authentication metrics— $D_{\text{all}}$ ,  $D_{\text{word}}$ , and  $D_{\text{letter}}$ —for images before and after editing in the `Instructpix2pix` [7] and `Imagic` [26] models, as the Semantic [39] and Vision [50] distances increase. Overall, we have observed a consistent trend where an increase in distance leads to a decrease in accuracy. This phenomenon can be primarily attributed to the extent of modifications made to the image during the editing process. As the alterations become more substantial, they tend to have a significantly greater impact on the effectiveness of the watermarks we have implemented.

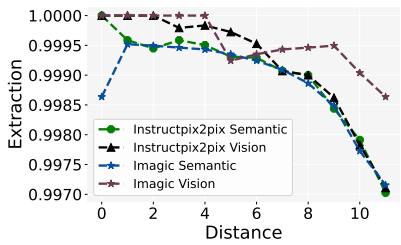


(a) Watermarking encoder weight  $\lambda$  difference with Instructpix2pix model.

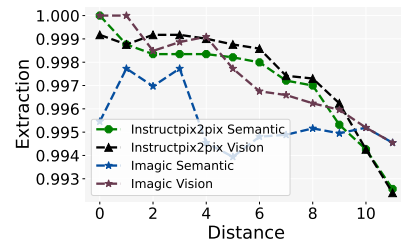


(b) Watermarking encoder weight  $\lambda$  difference with Imagic model.

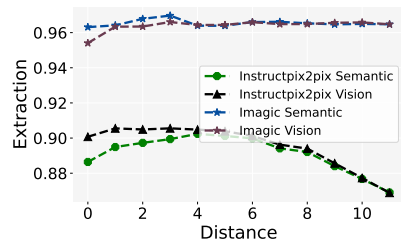
Figure 15: The trend in encoder loss weight for both Instructpix2pix and Imagic models, as observed in (a) and (b), reveals that at a minimal weight such as 128, watermarks become entirely invisible post-edit. Conversely, at lower weights like 1/128, watermarks become observable after editing. An optimal trade-off is found at a weight of 1/2, where watermarks typically remain unseen post-edit and yet have a high probability of being extracted by Ext.



(a)  $D_{\text{letter}}$  accuracy



(b)  $D_{\text{word}}$  accuracy



(c)  $D_{\text{all}}$  accuracy

Figure 16: The watermark extraction accuracy diminishes with increasing edit distance. As edit distance often correlates with the extent of image modifications, extensive edits lead to reduced preservation of the original image’s IP information, consequently diminishing IP infringement on the original image.